Research Square

Preprints are preliminary reports that have not undergone peer review.
They should not be considered conclusive, used to inform clinical practice,
or referenced by the media as validated information.

Light Transmission through Multilayer Metal Gratings with Periodic Slit Array Structures

Li Qun

liq@ecut.edu.cn

East China University of Technology

Fang Cheng

East China University of Technology

Chen Zhiming

East China University of Technology

Research Article

Keywords: Extraordinary optical transmission, Multilayer metal grating, Surface plasmon, Rigorous coupled-wave analysis, Slit array

Posted Date: September 15th, 2026

DOI: https://doi.org/10.21203/rs.3.rs-10848798/v1

License: This work is licensed under a Creative Commons Attribution 4.0 International License.
Read Full License

Additional Declarations: No competing interests reported.

Light Transmission through Multilayer Metal Gratings with Periodic Slit Array Structures

Li Qun*, Fang Cheng, Chen Zhiming

College of Science, East China University of Technology, Fuzhou, Jiangxi 344000, China

* Corresponding author. E-mail: [liq@ecut.edu.cn]

Abstract

We design a multilayer periodic metallic silver film grating with a slit array structure and investigate its electromagnetic transmission characteristics using the rigorous coupled-wave analysis (RCWA) method. The physical mechanism underlying the extraordinary optical transmission (EOT) phenomenon is elucidated through steady-state field distribution analysis. Our results reveal significant modifications in the transmission spectrum when transitioning from a single-layer to a multilayer grating configuration. Calculations of the steady-state electromagnetic field distribution demonstrate enhanced field coupling at transmission wavelengths associated with EOT. The magnetic field enhancement is attributed to surface plasmon resonance occurring both between adjacent silver film layers and within the slits. We conclude that the EOT behavior in metal grating slit arrays originates from the coupling resonance of surface plasmons at the metal–dielectric interface; under this resonance condition, the metallic silver film grating structure exhibits pronounced EOT.

Keywords: Extraordinary optical transmission · Multilayer metal grating · Surface plasmon · Rigorous coupled-wave analysis · Slit array

1 Introduction

Since Ebbesen and co-workers discovered extraordinary optical transmission (EOT) through metallic thin films perforated with two-dimensional periodic cylindrical hole arrays in 1998 [1], the transmission behavior of metallic gratings has attracted extensive theoretical and experimental interest. Studies have shown that when electromagnetic waves irradiate such periodic structures, the transmittance at specific wavelengths is substantially enhanced, exceeding the predictions of conventional aperture theory. Researchers have designed periodic grating structures of various geometries to explore the EOT phenomenon, including two-dimensional configurations such as periodic cylindrical and rectangular hole arrays [2], as well as one-dimensional structures such as slit arrays [3], annular apertures [4], single holes surrounded by periodic ripples [5], and apertureless plasmonic metagratings [6]. In recent years, EOT-based structures have also found emerging applications in plasmonic biosensing [7, 26], spectral filtering [8], and CMOS-compatible photodetection [9], further motivating the exploration of novel grating architectures.

The physical mechanism responsible for EOT has also been the subject of continuous investigation. The prevailing view attributes EOT to the interaction between incident electromagnetic waves and surface plasmon polaritons (SPPs) [10]. Specifically, SPPs can be excited when the in-plane wavevector component of the incident light matches the SPP dispersion relation via the grating reciprocal lattice vector. For normal incidence ($\theta = 0$), the phase-matching condition is given by

$$k_{\mathrm{SPP}} = mG = m\frac{2\pi}{D},$$

where $k_{\mathrm{SPP}} = (\omega/c)\sqrt{\varepsilon_m\varepsilon_d/(\varepsilon_m + \varepsilon_d)}$ is the SPP wavevector, ε_m and ε_d are the dielectric constants of the metal and surrounding dielectric, respectively, $G = 2\pi/D$ is the reciprocal lattice vector of the grating with period D, and m is an integer representing the diffraction order. When this phase-matching condition is satisfied, SPPs are excited and propagate through the slit apertures to the opposite surface of the metal, thereby giving rise to EOT [11, 12]. In addition, some researchers have proposed that localized surface plasmon (LSP) resonance also plays a crucial role in the EOT phenomenon [13, 14]. Recent work has further demonstrated that the interplay between SPPs, LSPs, and Fabry–Pérot-like waveguide resonances can lead to complex hybridized modes in plasmonic nanostructures [15, 16]. For instance, Hidayat et al. [15] observed dual plasmonic modes—long-range SPR and quasi-localized LSPR—in rectangular wave-shaped surface relief gratings, while Langevin et al. [16] reported intertwined Fano resonances in subwavelength metallic gratings that enable omnidirectional wideband optical transmission.

To date, investigations into the EOT of subwavelength slit array structures can be broadly categorized into three groups according to the number of metal layers and their geometric configurations. The first group comprises single-layer and double-layer planar metal film gratings. For double-layer structures, Chan et al. [17] demonstrated that evanescent field coupling between adjacent metal layers leads to surprisingly large transmission at particular wavelengths, even when no direct line of sight exists through the structure. More recently, Lei et al. [18] reported enhanced transmittance and Faraday rotation in double-layer metallic gratings, attributing the enhancement to interlayer plasmonic coupling, while Liu and Sun [8] showed that asymmetric bi-layer metallic nanoslit arrays can achieve narrow-band filtering with low sidebands through the coupling of local plasmon resonance and in-plane SPR modes. Although these double-layer studies have established the importance of interlayer coupling, they are inherently limited to two metal layers and cannot reveal how the transmission behavior evolves as the number of functional layers further increases.

The second group involves multilayer metallic structures with non-planar or non-uniform geometries. Gan and Gbur [19] investigated EOT through up to five layers of corrugated metallic thin films and found that the multilayer system can significantly impede field decay; however, their corrugated film geometry differs fundamentally from planar slit arrays, and the total metal thickness was limited to 500 nm with unequal layer thicknesses. Qi et al. [20] proposed sandwich-shaped multilayer tapered metallic slit arrays that achieve broadband infrared transmission through gradual impedance variation, but the tapered slit profile introduces geometric complexity that complicates the isolation of layer-count

effects. Liu et al. [21] reported tunable optical transmission in Au/Al multilayer slit gratings governed by field interference and Fabry–Pérot-like resonances, yet the use of dissimilar metals (Au/Al) introduces material heterogeneity as an additional variable.

The third group encompasses theoretical and computational method developments for multilayer plasmonic structures. The RCWA method has been widely adopted for the analysis of multilayer plasmonic nanostructures due to its computational efficiency and accuracy for periodic structures [22–24]. Schlipf and Fischer [22] applied RCWA to the design of multilayer plasmonic refractive index sensors, Pandey and Kumar [23] demonstrated quality-factor enhancement in plasmonic grating sensors using RCWA simulations, and Sassi et al. [24] extended RCWA to two-dimensional silicon carbide grating-based SPR gas sensors. While these studies showcase the versatility of RCWA for multilayer plasmonic systems, they focus primarily on sensor performance optimization rather than on the systematic evolution of EOT behavior with layer count.

Despite these advances, a systematic investigation of purely metallic, planar, equal-thickness multilayer slit gratings—where the total metal thickness is held constant while the number of layers varies from one to five—remains absent in the literature. Such a controlled design is essential because it isolates the effect of layer count and interlayer coupling from confounding variables such as total thickness variation, geometric tapering, and material heterogeneity. In particular, the evolution of transmission peak positions, intensities, and steady-state field distributions as the number of equal-thickness silver layers increases from two to five has not been thoroughly characterized.

In this study, we employ the RCWA method to systematically investigate the anomalous transmission behavior of two-dimensional metal grating structures consisting of one to five silver layers, with the total metal thickness held constant at 1000 nm and each layer having an equal thickness of 1000/n nm. We calculate the transmission spectra over the wavelength range of 1000–3000 nm and optimize the interlayer spacing for each layer count to maximize the EOT response. We further compute the steady-state electromagnetic field distributions within the grating layers and slit structures to elucidate the physical mechanisms underlying the anomalous transmission behavior. By comparing multilayer gratings with a single-layer reference of equal total thickness, we reveal how the number of layers systematically affects the transmission peak positions, intensities, and field localization patterns.

2 Model and computation

The two-dimensional multilayer metal grating structure investigated in this work is schematically illustrated in Fig. 1. The metal film consists of silver (Ag) and is surrounded by air. Each silver film has a fixed thickness H/n, where n is the number of layers and the total metal thickness is 1000 nm. The grating has a fixed periodicity of $D = 1000$ nm along the x-direction, a slit width of $a = 100$ nm, and a variable interlayer spacing G. For clarity, only a three-layer grating structure is depicted in Fig. 1. The multilayer metal grating is a two-dimensional structure, with the z-direction representing the direction of electromagnetic wave incidence. The incident light is transverse-magnetic (TM) polarized, with the magnetic field oriented along the y-direction.

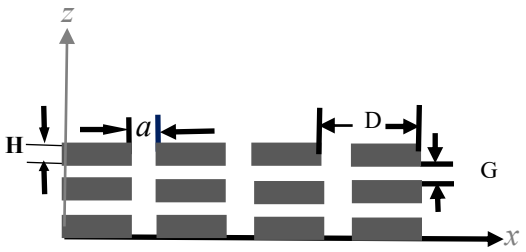
The dielectric constant of silver is described by the Drude model:

$$\varepsilon(\omega) = \varepsilon_\infty - \frac{\omega_p^2}{\omega^2 + i\gamma\omega}$$

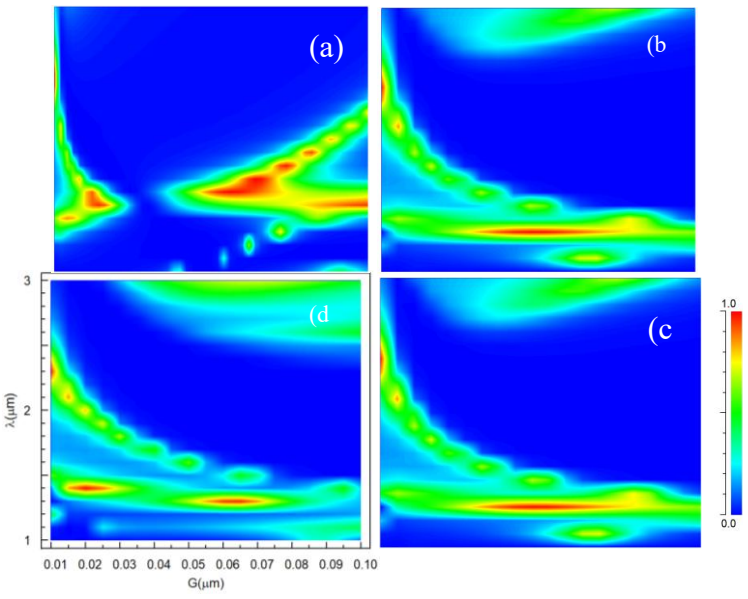
where ε_∞ is the high-frequency dielectric constant, ω_p is the plasma oscillation frequency, γ is the damping coefficient, and ω is the angular frequency of the incident electromagnetic wave [25]. The Drude parameters used in this work are $\varepsilon_\infty = 3.7$, $\hbar\omega_p = 9.1$ eV, and $\hbar\gamma = 0.048$ eV, consistent with values commonly employed for silver in the near-infrared regime.

The interlayer spacing G is not fixed a priori. Instead, we perform a scan over a range of wavelengths and spacings and identify the approximate matching values at which the electromagnetic field transmission intensity reaches its maximum, as shown in Fig. 2. For n = 2, 3, 4, and 5, corresponding to double-layer, triple-layer, quadruple-layer, and quintuple-layer metal gratings, respectively, the optimized spacings are 150 nm, 100 nm, 40 nm, and 20 nm.

All numerical simulations are performed using the RCWA method with 21 retained Fourier diffraction orders (i.e., orders from -10 to $+10$), which was verified to be sufficient for convergence of both the transmission coefficient and the electromagnetic field distributions. A convergence test showed that increasing the number of retained orders beyond 21 changed the calculated transmittance by less than 0.1%. The transmission coefficient is calculated as the ratio of the transmitted power to the incident power in the zeroth diffraction order.



[Figure 1: Schematic of the multilayer silver film slit array structure. The grating period is D, the slit width is a, each metal layer has thickness H/n, and the interlayer spacing is G.]

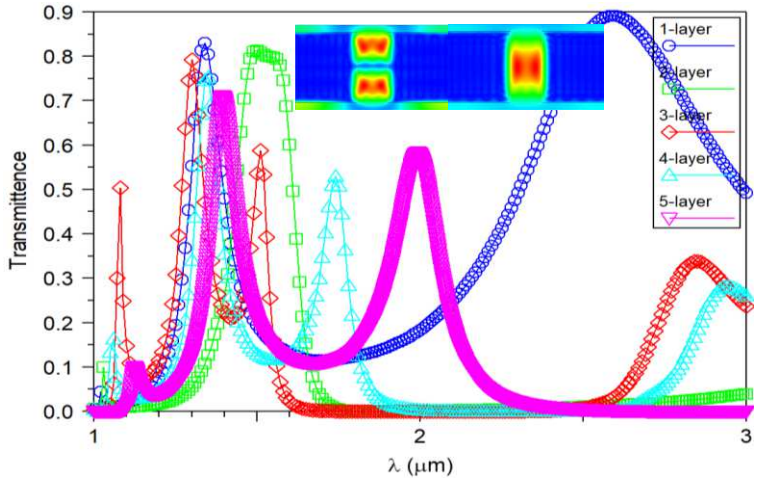


[Figure 2: Relationship between wavelength, silver film spacing, and transmission intensity for (a) 2-layer, (b) 3-layer, (c) 4-layer, and (d) 5-layer gratings.]

3 Results and discussion

3.1 Transmission spectra

Figure 3 presents the transmission spectra of multilayer gratings as a function of incident wavelength. The thickness of each metal grating layer is given by H = 1000/n nm, such that the total thickness of the multilayer film remains constant at 1000 nm. A single-layer structure with a thickness of 1000 nm is used as a reference for comparison with the multilayer grating structures.



[Figure 3: Transmission spectra of the multilayer silver film slit array structure for different numbers of layers.The inset shows the steady-state magnetic field distribution of the single-layer grating at λ = 1340 nm and 2590nm]

As shown in Fig. 3, the 1000 nm single-layer metal grating exhibits transmission peaks at wavelengths of 1340 nm and 2590 nm. The peak at 1340 nm is sharper than that at 2590 nm, and a weak transmission peak with a transmittance of less than 5% appears at 1020 nm.

When the single-layer metal grating is divided into two equal-thickness 500 nm layers (double-layer grating), a broader peak band emerges in the transmission spectrum from approximately 1500 nm to 1550 nm. This peak band is red-shifted relative to the secondary maximum of the single-layer grating at 1340 nm, while the broad peak originally located at 2590 nm disappears within the calculated wavelength range of 1000–3000 nm.

For the three-layer grating, in which each layer has a thickness of 1000/3 nm, four transmission peaks appear at wavelengths of 1080 nm, 1300 nm, 1510 nm, and 2850 nm. The transmittance at 1080 nm reaches approximately 50%, consistent with EOT behavior. The peaks at 1300 nm and 1510 nm appear to originate from the splitting and red-shifting of the single-layer peak at 1340 nm, while the broad peak at 2850 nm seems to be a red-shifted counterpart of the single-layer peak at 2590 nm, albeit with reduced intensity (transmittance of 34%).

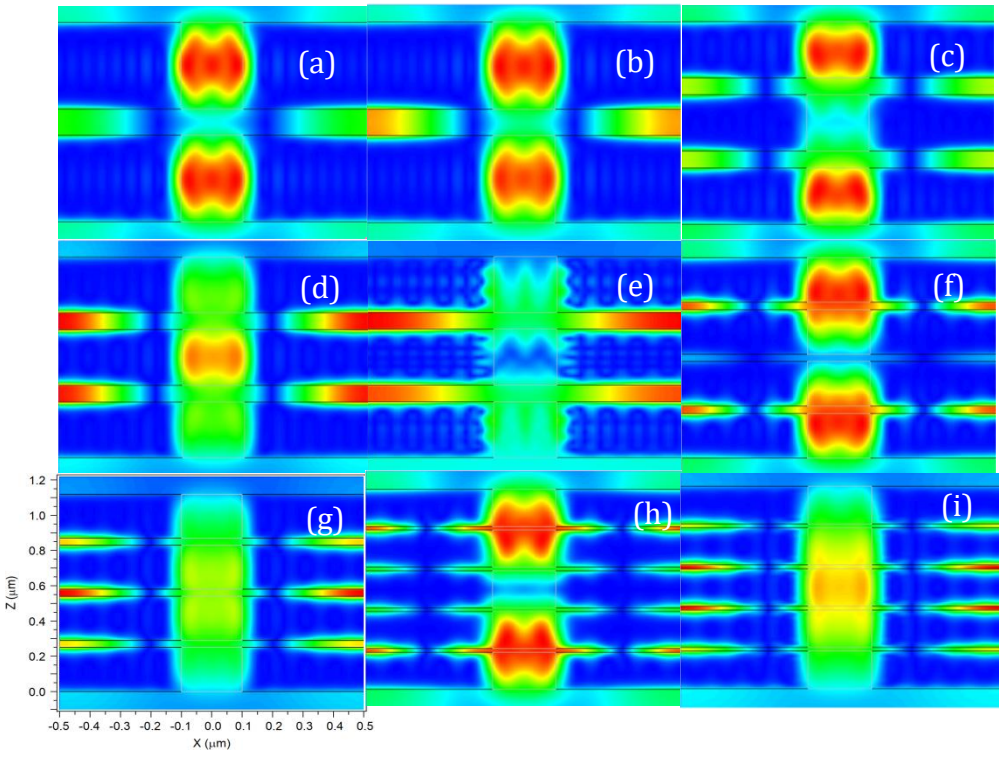
Similar to the three-layer grating, the four-layer structure exhibits relatively sharp transmission peaks at 1350 nm and 1740 nm, along with a broad peak at 2940 nm with a transmittance of approximately 28%. The five-layer structure displays sharp peaks at 1400 nm and 1990 nm.

Comparing the transmission spectra of the multilayer gratings with that of the 1000 nm single-layer grating, several trends emerge. First, the overall transmission intensity does not decrease significantly as the number of grating layers increases, despite the presence of additional metal–air interfaces. This observation is consistent with the findings of Gan and Gbur [19], who reported that multilayer metallic systems can exhibit transmission greater than that expected from simple Fabry–Pérot-like behavior due to plasmon-assisted field propagation. Second, the single-layer peak at 1340 nm tends to split into multiple transmission peaks as the number of layers increases, and the peak positions gradually shift toward longer wavelengths. This peak-splitting behavior is consistent with previous observations in multilayer plasmonic structures [8, 21], where increasing the number of functional layers introduces additional coupling modes. Third, the broad peak at 2590 nm—where the single-layer structure reaches its maximum transmission—exhibits decreasing intensity and eventually disappears as the number of layers increases. At all transmission peaks, the transmittance substantially exceeds the ratio of the slit area to the period area (100/1000 = 10%), confirming the occurrence of EOT.

The observed transmission peaks can be further understood in the context of the SPP phase-matching condition discussed in the Introduction. For the grating period $D = 1000$ nm used in this work, the first-order SPP resonance ($m = 1$) satisfies $k_{\mathrm{SPP}} = 2\pi/D = 6.28 \times 10^{-3}$ nm^{-1}. For silver in the near-infrared regime, this wavevector corresponds to resonant wavelengths on the order of 1–3 μm, consistent with the observed peaks at 1340 nm and 2590 nm for the single-layer grating. The weaker feature at 1020 nm may be attributed to a higher-order SPP mode or a Wood anomaly. As the number of metal layers increases, the introduction of additional metal–dielectric interfaces modifies the effective dielectric environment experienced by the SPPs, leading to a progressive redshift of the resonant wavelengths. Furthermore, the interlayer evanescent coupling creates new hybridized plasmonic modes, which manifest as the observed peak splitting into multiple sub-peaks. The broad peak at longer wavelengths (2590 nm for the single layer) is associated with a Fabry–Pérot-like waveguide resonance inside the slits; as the layer count increases, the reduced individual layer thickness and the interlayer coupling disrupt this waveguide resonance, leading to its diminished intensity and eventual disappearance from the calculated spectral range.

3.2 Steady-state magnetic field distribution and physical mechanism

To further elucidate the physical mechanism of EOT, we calculate the spatial distribution of the steady-state magnetic field (Hz). The spatial magnetic field distribution of the single-layer grating structure is shown in the inset of Fig. 3. At incident wavelengths of 1340 nm and 2590 nm, local resonances are formed inside the slit. Notably, at 1340 nm, two resonant modes are observed, whereas at 2590 nm, only one mode is present, corresponding to the maximum transmission intensity. The resonant modes are symmetric both vertically and horizontally, originating from surface plasmon coupling resonance generated on the metal surfaces on both sides of the slit. At these wavelengths, the silver film slit structure resembles a Fabry–Pérot waveguide resonant cavity: the incident electromagnetic wave induces surface plasmon coupling resonance on the two surfaces of the slit, which can also be interpreted as magnetic field local waveguide resonance. This coexistence of SPP-mediated and waveguide-mediated transmission channels has been previously noted in single-layer metallic grating systems [10, 15].



[Figure 4: Magnetic field distribution of the multilayer silver film slit array structure at different incident wavelengths. Panels (a)–(i) correspond to the transmission peaks identified in Fig. 3.]

The spatial magnetic field distributions for the multilayer grating structures are presented in Fig. 4. Panels (a) through (i) correspond to the magnetic field intensity distributions at the transmission peaks identified in Fig. 3.

For the double-layer grating, panels (a) and (b) correspond to the transmission peak band from approximately 1500 nm to 1550 nm. The magnetic field distributions at these two wavelengths are qualitatively similar, with the transmission intensity at 1550 nm being slightly weaker than that at 1500 nm. The field distribution reveals that coupling resonance of surface plasmons is formed between the two layers at 1550 nm. This interlayer coupling is consistent with the mechanism described by Chan et al. [17] and Lei et al. [18], who attributed enhanced transmission in double-layer gratings to evanescent field coupling between adjacent metal layers.

For the three-layer structure, panels (c), (d), and (e) show the steady-state magnetic field distributions. At 1300 nm, where the transmittance is highest, two resonant modes with vertical and horizontal symmetry are formed between the slits of the first and third layers, respectively. At 1080 nm and 1510 nm—corresponding to the two sub-peaks—a lower-intensity resonant mode is formed between the slits of the second layer, while strong local coupling resonances occur between the first and second layers and between the second and third layers.

Similar behavior is observed in the four-layer grating structure. As shown in panels (f) and (g), at the maximum transmission peak wavelength of 1350 nm, strong coupling resonance occurs within the slits, producing two vertically and horizontally symmetric resonant modes. A relatively weaker coupling resonance is observed between the second and third layers.

The five-layer grating structure, shown in panels (h) and (i), exhibits analogous behavior: strong coupling resonance within the slits produces two resonant modes, while at the wavelength of 1740 nm, resonant modes form between the second and third layers and between the third and fourth layers.

From these observations, we infer that the steady-state magnetic field distribution in multilayer silver film slit arrays exhibits vertically and horizontally symmetric resonant modes due to the coupling resonance of surface plasmons on the silver surface. The steady-state field distribution at the maximum transmission peak is localized within the slits, driven by surface plasmon resonance, whereas the resonant magnetic field distribution at the sub-peaks occurs between the grating silver films. The progressive splitting of transmission peaks with increasing layer number can be understood as a consequence of the increasing number of coupled plasmonic cavities, which gives rise to additional hybridized resonance modes. This mode hybridization mechanism is consistent with recent studies of multilayer plasmonic structures, where interlayer coupling has been shown to generate new resonant modes and modify the spectral response [8, 19, 21].

4 Conclusion

In this study, we have investigated the extraordinary optical transmission behavior of electromagnetic waves through multilayer grating structures based on silver film slit arrays, with the aim of elucidating the physical mechanism of the EOT phenomenon. Using the RCWA method, we have compared the EOT behavior of single-layer and multilayer film grating slit arrays. The multilayer gratings were designed such that each layer has an equal thickness of H/n (where n is the number of grating layers), while the total thickness remains constant at 1000 nm and the slit width is fixed at 100 nm.

Our analysis of the transmission spectra from single-layer to multilayer slit arrays reveals significant differences between single-layer and multilayer gratings. As the number of layers increases, the transmission peak at 1340 nm in the single-layer structure gradually redshifts and splits into two or three transmission peaks in the multilayer configurations. Meanwhile, the broad transmission peak at 2590 nm exhibits decreasing intensity and eventually disappears as the number of layers increases.

Further calculations of the steady-state field distribution indicate that enhanced electromagnetic field coupling occurs at the transmission wavelengths where EOT is observed. Analysis of the magnetic field enhancement reveals that it originates from surface plasmon resonance on the metal surface. Therefore, we conclude that the EOT behavior of metal grating slit array structures arises from the coupling resonance of surface plasmons at the metal–dielectric interface, and that EOT occurs only when this resonance condition is satisfied.

These findings contribute to a more detailed understanding of EOT mechanisms in purely metallic multilayer grating structures and may inform the design of subwavelength optical devices such as plasmonic filters, sensors, and modulators based on multilayer metal structures. Future work could explore the effects of varying the slit width, grating period, and interlayer spacing on the transmission characteristics, as well as experimental fabrication and characterization of the proposed structures.

This research did not receive funding.

References

1. T.W. Ebbesen, H.J. Lezec, H.F. Ghaemi, T. Thio, P.A. Wolff, Nature **391**, 667 (1998)
2. J.A. Porto, F.J. García-Vidal, J.B. Pendry, Phys. Rev. Lett. **83**, 2845 (1999)
3. F.J. García-Vidal, L. Martín-Moreno, H.J. Lezec, T.W. Ebbesen, Phys. Rev. Lett. **90**, 213901 (2003)
4. H.F. Ghaemi, T. Thio, D.E. Grupp, T.W. Ebbesen, H.J. Lezec, Phys. Rev. B **58**, 6779 (1998)
5. Y. Takakura, Phys. Rev. Lett. **86**, 5601 (2001)
6. S.K. Verma, S.K. Srivastava, Appl. Phys. Lett. **122**, 171705 (2023)

7. Z. Zhang, F. Zhao, R. Gao, C.-Y. Jao, C. Ma, J. Li, X. Li, B.-O. Guan, A.E. Cetin, K. Chen, Nanophotonics **11**, 507 (2022)

8. H. Liu, Z. Sun, Opt. Express **29**, 13590 (2021)

9. W. Han, S. Reiter, J. Schlipf, C. Mai, Opt. Express **31**, 17389 (2023)

10. L. Martín-Moreno, F.J. García-Vidal, H.J. Lezec, K.M. Pellerin, T. Thio, J.B. Pendry, T.W. Ebbesen, Phys. Rev. Lett. **86**, 1114 (2001)

11. F.J. García-Vidal, L. Martín-Moreno, Phys. Rev. Lett. **87**, 246801 (2001)

12. H. Liu, P. Lalanne, M.P. van Exter, Phys. Rev. B **72**, 155409 (2005)

13. A.G. Brolo, E. Arctander, R. Gordon, B. Leathem, K.L. Kavanagh, Nano Lett. **4**, 2015 (2004)

14. J.N. Anker, W.P. Hall, O. Lyandres, N.C. Shah, J. Zhao, R.P. Van Duyne, Nat. Mater. **7**, 442 (2008)

15. R. Hidayat, J.S. Pradana, A. Fariz, S. Komalasari, S. Chalimah, H. Bahar, Sci. Rep. **13**, 30083 (2023)

16. D. Langevin, J. Jaeck, R. Haïdar, P. Bouchon, Opt. Lett. **49**, 6665 (2024)

17. H.B. Chan, Z. Marcet, K. Woo, D.B. Tanner, D.W. Carr, J.E. Bower, R.A. Cirelli, E. Ferry, F. Klemens, J. Miner, C.S. Pai, J.A. Taylor, Opt. Lett. **31**, 516 (2006)

18. C. Lei, Z. Man, S. Tang, Appl. Phys. Express **13**, 122002 (2020)

19. C.H. Gan, G. Gbur, Opt. Express **17**, 20553 (2009)

20. Y. Qi, X. Zhang, P. Zhou, C. Yan, X. Wang, Sci. China Phys. Mech. Astron. **48**, 074201 (2018)

21. H. Liu, Y. Li, Z. Sun, J. Opt. **14**, 055003 (2012)

22. J. Schlipf, I.A. Fischer, Opt. Express **29**, 36201 (2021)

23. A.K. Pandey, H. Kumar, Opt. Quantum Electron. **55**, 57 (2023)

24. I.A. Sassi, M.B.E.H. Rhouma, M.G. Daher, Opt. Quantum Electron. **55**, 880 (2023)

25. P.B. Johnson, R.W. Christy, Phys. Rev. B **6**, 4370 (1972)

26. S. Afsheen, T. Iqbal, M. Shakil, A. Bashir, M. Usman, M. Ijaz, Opt. Quantum Electron. **52**, 123 (2020)